FRONTIERS OF PHYSICS

RESEARCH ARTICLE
Volume 21 / Issue 11 / 112201 / 2026

Formation and evolution of filtered solitons in figure-9 mode-locked fiber lasers

Wenfeng Luo[1], Yumeng Cao[1], Xiaohui Li[2,†], Shuyuan Lv[1], Yerou Wang[1], Fei Xi[3]

1 School of Electronic Engineering, Xi'an University of Posts and Telecommunications, Xi'an 710121, China
2 School of Physics & Information Technology, Shaanxi Normal University, Xi'an 710062, China
3 Shaanxi Runchenglai Optoelectronic Technology Co., Ltd., Xianyang 712023, China
Corresponding author. E-mail: †lixiaohui@snnu.edu.cn
Received December 3, 2025; accepted February 13, 2026

ABSTRACT

An erbium-doped filtered mode-locked fiber laser is demonstrated in this work. Mode-locked operation was achieved using the nonlinear amplifying loop mirror (NALM) technique incorporating a filtering effect. The proposed fiber laser employs a 1.8 m polarization-maintaining fiber (PMF) in the NALM loop, yielding a free spectral range (FSR) of 3.6 nm. The high birefringence of the PMF was utilized for optical filtering to construct the fiber laser. Stable filtered soliton pulses were obtained with a central wavelength of 1566 nm. Upon increasing the pump power to 304 mW and precisely adjusting the polarization controller, filter-induced noise-like solitons centered at 1562.6 nm were generated. This passively mode-locked fiber laser features a simple structure and stable performance, enabling switchable operation between two filtered soliton states, and thus holds significant application potential in fields such as all-optical communication.

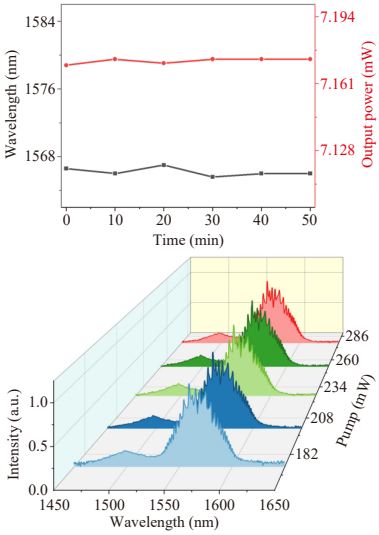

Keywords Sagnac, filtered soliton, figure-9 fiber laser, erbium-doped fiber laser

1 Introduction

Mode-locked fiber lasers have emerged as a highly effective means of generating stable ultrashort pulses, owing to their compact structure, high efficiency, and superior beam quality [1]. Passively mode-locked fiber lasers are extensively employed in a variety of fields, including lidar [2, 3], fiber-optic sensing [4], material processing [5], and medical applications [6, 7]. Current passive mode-locking mechanisms can be broadly classified into two categories: material-based saturable absorbers [8, 9, 36] and artificial saturable absorbers.

Artificial saturable absorbers can be implemented through various technical schemes, including nonlinear polarization rotation (NPR) [10, 11], the nonlinear optical loop mirror (NOLM) [12, 13], and the nonlinear amplifying loop mirror (NALM) [14, 15]. Among these, NALM and NPR are recognized for their high damage threshold [14], large modulation depth, and fast response time [16], making them suitable for generating high-performance femtosecond pulses [17, 18]. In 2024, Kitajima et al. demonstrated an all-polarization-maintaining figure-9 cavity erbium-doped fiber laser [17]. The integration of a non-reciprocal phase shifter into the cavity enhances the self-starting capability of the mode-locking mechanism, while the laser simultaneously exhibits high environmental stability. Compared with NPR, passively mode-locked fiber lasers based on NALM offer distinct advantages, including full compatibility with polarization-maintaining

https://doi.org/10.15302/frontphys.2026.112201

systems [14], which significantly improves the overall environmental stability [19]. Notably, the figure-of-nine passively mode-locked fiber laser incorporating an integrated phase shifter [20] enables the reliable generation of mode-locked pulses characterized by a high repetition rate [21], narrow pulse width, and low noise [22]. Moreover, it achieves self-starting operation [23] and ensures long-term stability [37], thereby providing a reliable foundation for practical applications.

The Sagnac loop is based on the Sagnac effect and functions as a filter by leveraging the phase difference generated between clockwise and counterclockwise propagating light in a circular optical path [24, 25]. It features a simple and compact structure, flexibly tunable filtering characteristics [26], low sensitivity to environmental perturbations [27], and seamless integration into all-fiber systems [28]. By judiciously designing the parameters of the Sagnac loop, such as the fiber length and coupler splitting ratio, selective transmission or reflection of light at specific wavelengths can be achieved, effectively suppressing noise and stray light in the spectrum while enabling high-precision spectral shaping and wavelength selection. As a result, it holds great potential for applications in spectral optimization of ultrafast pulse fiber lasers [29], wavelength demodulation in fiber-optic sensing systems [30], and channel selection in optical communication systems [38].

In ultrafast pulse fiber lasers, a filtered soliton represents a distinct pulse regime formed by the interplay among filtering, fiber nonlinear effects, and dispersion. Its defining characteristic is a narrowed pulse spectrum, which enables stable propagation in both the time and frequency domains. In contrast to conventional solitons, which are primarily shaped by dispersion and nonlinearity, filtered solitons are predominantly governed by filtering effects during nonlinear evolution. Consequently, they find extensive application in high-power, narrow-bandwidth ultrafast pulse sources.

This study presents an erbium-doped fiber laser that integrates a figure-9 cavity with a Sagnac loop. By exploiting the structural properties of the figure-9 cavity based on a NALM and incorporating the filtering effect of the Sagnac loop, we constructed a fiber laser capable of generating stable mode-locked pulses. Leveraging the high birefringence of polarization-maintaining fiber, optical filtering of the mode-locked pulses was achieved, with an operating threshold of 200 mW and an unlocking threshold of 6 mW. When the pump power was reduced to 20.6 mW, stable filtered soliton pulses were successfully generated, exhibiting a central wavelength of 1566 nm. The laser yielded an output power of 7.173 mW, a repetition rate of 13.5 MHz, a pulse interval of 74 ns, and a SNR of 63 dB. Upon increasing the pump power to 304 mW and further fine-tuning the PC, an evolving filtered soliton pulse was generated. The resulting filter-induced noise-like soliton exhibited a central wavelength of 1562.6 nm, a 3-dB bandwidth of 9.8 nm, and an SNR of 52 dB. This passively mode-locked fiber laser features a simple device structure, stable output characteristics, and holds significant potential for engineering applications in fields such as all-optical communication systems.

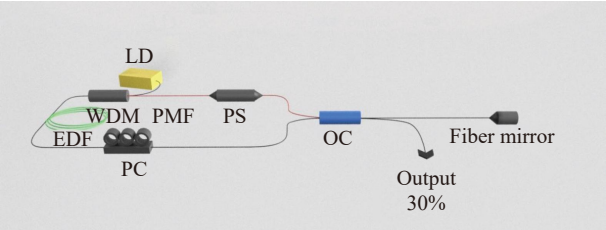

Fig. 1 Schematic diagram of the laser experimental setup.

2 Experimental setup and principle

A schematic of the proposed figure-9 passively mode-locked fiber laser based on a Sagnac loop is shown in Fig. 1. The resonator, designed with consideration of modulation depth and threshold pump power, consists of a NALM and a linear arm, which are interconnected via a 2×2 optical coupler (OC) with a coupling ratio of 70:30. The NALM loop, located on the left side of the OC, comprises a 3.5 m erbium-doped fiber (EDF), a polarization-maintaining phase shifter (PS), a PC, and a wavelength-division multiplexer (WDM). The PC is utilized to adjust the polarization state and phase of the light, whereas the PS introduces a fixed $\pi/2$ phase shift. A 976 nm laser diode serves as the pump source and is coupled into the cavity via a 976/1550 nm WDM. The pigtail of the polarization-maintaining PS is a 1.8 m PM1550 polarization-maintaining fiber, and a NALM loop incorporating a Sagnac filtering effect is thereby established. All other component pigtails are single-mode fibers (SMF-28e). On the right side of the 2×2 OC, a fiber mirror connected to the 70% port reflects approximately 98% of the light back into the cavity, while the remaining 30% port functions as the laser output. The group velocity dispersion (GVD) parameters of the EDF and SMF are 12 ps^2/km and –23 ps^2/km, respectively, and the total cavity length is approximately 15 m.

An optical spectrum analyzer (Anritsu MS9710C) was used to observe the real-time changes in the center wavelength and spectral width of the laser pulses, as well as to record and collect the spectral data. A 1 GHz digital oscilloscope (Rigol DS6104) was employed to observe the variation in the output pulses and record/collect data on pulse trains and single pulses. A 6 GHz RF analyzer (Rohde & Schwarz FSC6) was used to detect the repetition rate of the intracavity pulse signals to monitor the stability of the output pulses.

In the filter spectrum, the wavelength interval

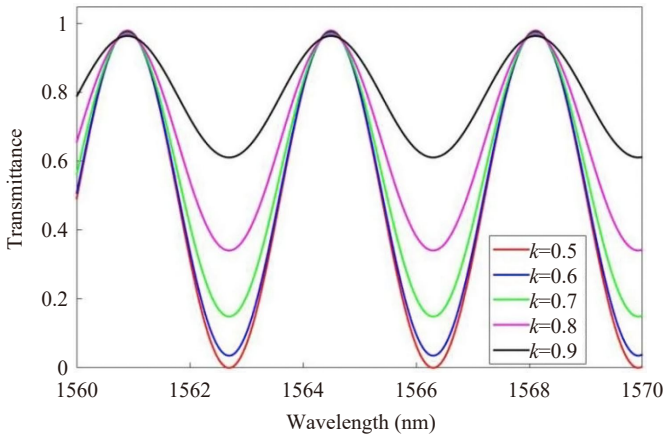

Fig. 2 Relationship between transmittance and wavelength under different coupling ratios.

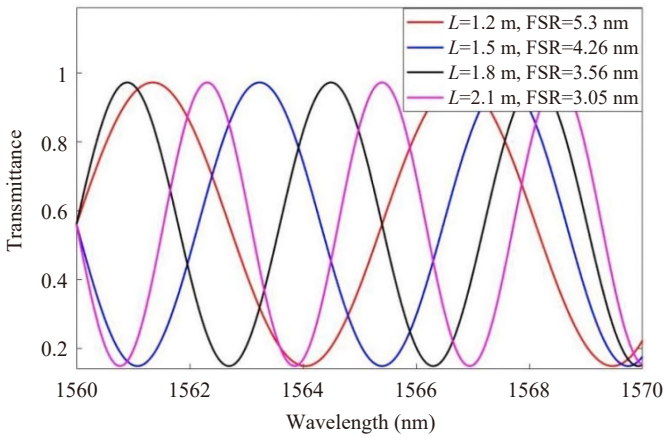

Fig. 3 Relationship between wavelength and transmittance for different lengths of PMF.

between two adjacent valleys—calculated as the difference between their corresponding wavelengths — represents the free spectral range (FSR) of the filter. It is expressed by Eq. (1) [31]:

$$\mathrm{FSR} = \frac{\lambda^2}{BL}, \tag{1}$$

where B is the birefringence of the polarization-maintaining fiber, L is the length of the polarization-maintaining fiber, and λ is the operating wavelength of the filter.

The Sagnac loop in this fiber laser acts as a filter, enabling the fine filtering of the pulse spectrum passing through the ring cavity. When the pulse travels through the PMF, the phase delay accumulated by adjusting the intracavity polarization state via the PC is denoted as $\Delta\varphi$:

$$\Delta\varphi = \frac{2\pi BL}{\lambda}. \tag{2}$$

In our experiment, the birefringence of the PMF is 3.77×10^{-4}, and the length of the PMF is 1.8 m.

The Sagnac filter in the experiment was composed of a 2×2 OC with a 70:30 splitting ratio, PC, and PMF. Without considering the inherent loss of the device itself, the Jones matrix expression for the OC is denoted as J_{OC}[32]:

$$J_{\mathrm{OC}} = \begin{pmatrix} \sqrt{1-k} & \mathrm{i}\sqrt{k} \\ \mathrm{i}\sqrt{k} & \sqrt{1-k} \end{pmatrix}, \tag{3}$$

where k is the coupling coefficient of the OC with the value of 0.7.

Based on Eqs. (1) to (3) and combined with the parameters of the components used in the fiber laser construction process, the overall transmittance function of this fiber laser can be derived as follows:

$$T = (1-k)^2 + k^2R^2 + 2k(1-k)R\cos\left(\Delta\varphi + \frac{\pi}{2}\right), \tag{4}$$

where R represents the reflectivity of the fiber mirror with the value of 0.98, and $\frac{\pi}{2}$ is the fixed phase shift provided by the phase shifter.

When the pulse enters the Sagnac loop through the 2×2 OC, the laser propagates in clockwise and counterclockwise directions. After passing through the PC and PMF separately, the lasers from the two directions enter the OC again, resulting in interference. Numerical simulations were conducted, and the relationship between transmittance and wavelength is shown in Fig. 2. When the coupling ratios are 0.5, 0.6, 0.7, 0.8, and 0.9, the transmittance exhibits periodic oscillations with changes in wavelength, which is a typical interference phenomenon. It can also be observed that the period remains unchanged for different coupling ratios, as shown in Fig. 2. This is because the period is determined by factors such as the optical path difference of the loop structure, and the coupling ratio does not change the period. From 0.5 to 0.9, the amplitude of the extreme points (peaks and valleys) of the transmittance changes significantly. When the coupling ratio is 0.9, the transmittance curve is relatively flat, with a weak interference effect and low modulation depth. As k decreased, the oscillation amplitude of the transmittance gradually increased, indicating a stronger interference effect and higher modulation depth.

Figure 3 shows the variation in transmittance with wavelength when the PMF lengths are 1.2, 1.5, 1.8, and 2.1 m. As the PMF length increased, the FSR gradually decreased. The FSR is related to the optical path difference of the Sagnac loop, and the optical path difference increases with increasing PMF length. This is consistent with Eq. (1), which shows the FSR is inversely proportional to the PMF length. This conclusion is helpful for analyzing the influences of the relevant PMF parameters and the

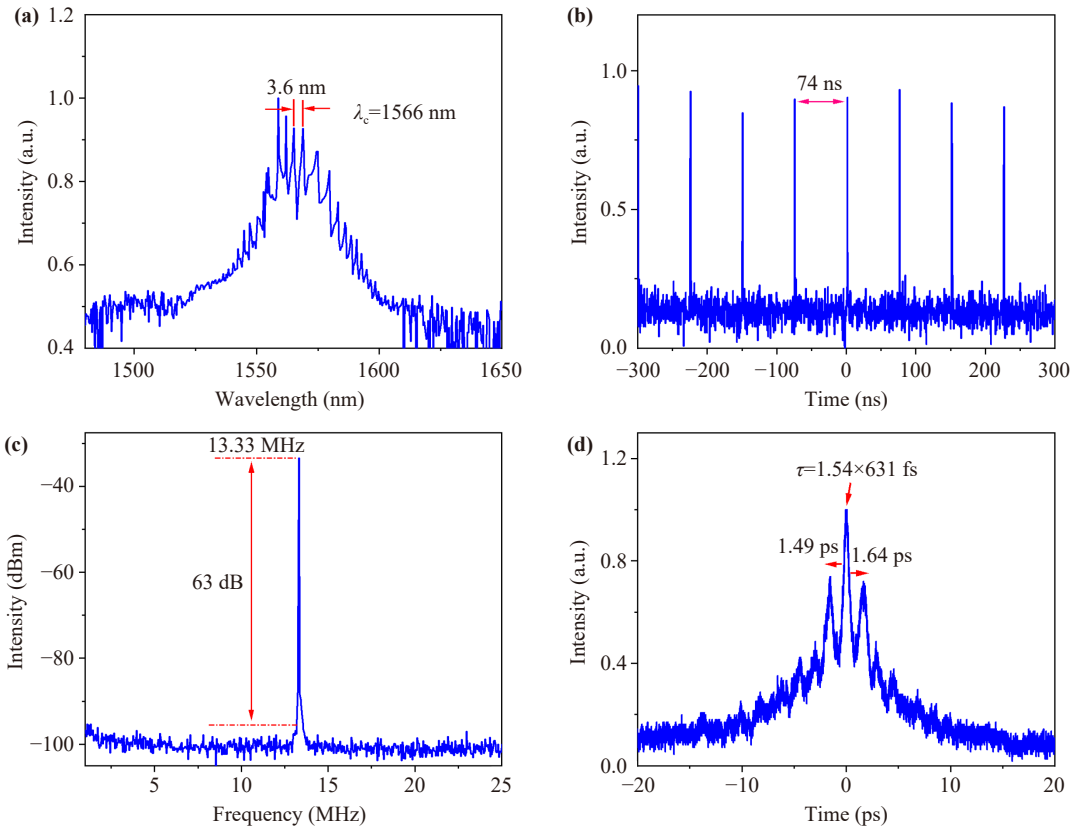

Fig. 4 Output pulse characteristics of the Sagnac loop with a 1.8 m PMF. **(a)** Spectrum; **(b)** Pulse train; **(c)** Radio Frequency spectrum; **(d)** Autocorrelation curve.

coupling ratio of the OC on the Sagnac loop transmittance.

3 Experimental results and discussion

Under standard experimental conditions with a pump wavelength of 976 nm, pulse self-starting was achieved at a pump power of 200 mW. When the pump power was decreased to 20.6 mW, a stable filtered soliton was formed; however, mode-locking was lost when the power was further reduced to 6 mW. A 1.8 m section of polarization-maintaining fiber (PMF) was integrated into the nonlinear amplifying loop mirror (NALM) to form the Sagnac loop. Figure 4(a) presents the output spectrum, which exhibits a central wavelength of 1566 nm and a free spectral range (FSR) of 3.6 nm. The high birefringence of the PMF induces a significant phase difference between the fast and slow axis modes as light propagates through the loop, resulting in high-contrast interference fringes and sharp spectral sidebands. Figure 4(b) presents the oscilloscope trace of the output pulse train. The measured time interval between adjacent pulses is 74 ns, corresponding to a fundamental repetition rate of 13.5 MHz, which agrees well with the cavity length of 15 m. The uniform pulse intensities observed on the oscilloscope indicate stable pulse operation. Figure 4(d) presents the autocorrelation trace of the output filtered soliton. Six lower-intensity peaks are symmetrically distributed on either side of the central peak, which exhibits a pulse width of 631 fs. The distances between the central peak and the adjacent lower-intensity peaks are 1.49 ps and 1.64 ps, respectively. The uniform birefringence distribution in the PMF leads to linear accumulation of phase differences between the clockwise and counterclockwise propagating waves, ultimately producing symmetric interference fringes in the frequency domain at the coupler. According to the Fourier transform duality principle, such symmetric frequency-domain modulation corresponds to symmetric sidelobe structures in the time domain. The filtering process disrupts the Fourier transform symmetry, causing the time-domain pulse to deviate from the standard sech^2 shape and potentially exhibit features such as steep edges or trailing tails. The symmetrically distributed low-amplitude peaks represent temporal sidelobes induced by the filtering effect. These structures are not independent solitons but rather inherent sidelobe features of the same filtered soliton pulse, with their symmetry arising from the modulation characteristics of the Sagnac filter in the frequency domain. Further analysis of the RF spectrum, shown in Fig. 4(c), reveals a SNR of 63 dB, confirming that the proposed fiber laser

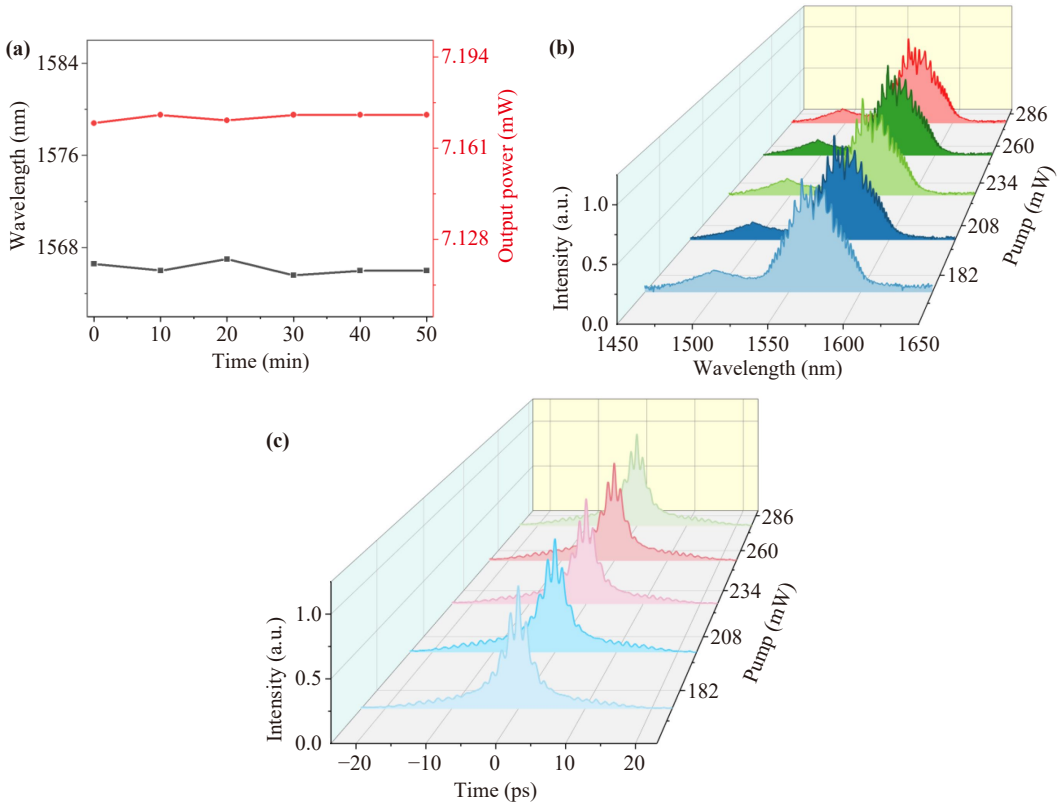

Fig. 5 Output stability of the Sagnac-Filtered pulses with a 1.8 m PMF. **(a)** Stability measurement of central wavelength and output power; **(b)** Evolution diagram of spectrum with pump power; **(c)** Evolution of autocorrelation trace with pump power.

operates stably with excellent mode-locking performance.

A filtered soliton is a type of "non-ideal soliton" formed by introducing an additional filtering mechanism based on the formation conditions of traditional solitons. When the seed pulse propagates in the cavity, the high-frequency or low-frequency components at the edges of its broad spectrum are truncated, and the spectrum is narrowed into a shape within the filtering bandwidth. As the filtered pulse continues to propagate, the SPM effect attempts to broaden the spectrum again; however, the filter truncates the newly generated edge components once more during the next round trip [33]. This process is repeated, and the stability condition shifts from the GVD-SPM balance to the GVD-SPM-filtering triple balance, where filtering becomes a key factor in suppressing spectral broadening and maintaining pulse stability.

To verify the temporal stability of the proposed mode-locked fiber laser, the central wavelength and output power were recorded every 10 minutes at a pump power of 20.6 mW, as shown in Fig. 5(a). Over a 50-minute period, the central wavelength and output power varied by only 0.6 nm and 0.003 mW, respectively, indicating no significant fluctuations and confirming stable pulse operation. The PC in the cavity was held at a fixed rotation angle while the pump power was gradually increased in 30 mW increments. Figure 5(b) illustrates the spectral evolution as the pump power was raised from 174 mW to 278 mW. Throughout this power range, the spectral sidebands remained largely unchanged, indicating that the cavity maintained a stable state with no substantial alterations in gain characteristics or intracavity optical conditions. This observation underscores the robustness of the laser design against environmental variations. As shown in Fig. 5(c), with the pump power increasing from 174 mW to 278 mW, the pulse width of the central peak remained essentially constant, and the temporal separation between the central peak and the two low-intensity side peaks also stayed nearly unchanged. These results confirm that the system operated in a stable mode-locked soliton regime. Within this specific power range, increasing the pump power primarily enhanced the pulse energy and peak power, while the pulse width remained constant, leading only to an increase in the intensity of the side lobes. The invariant temporal separation between the side peaks and the central peak is attributed to the fact that this spacing is determined by the cavity round-trip time, which is independent of the pump power.

When the pump power was increased to 291.6 mW, the output spectrum evolved as the PC was adjusted.

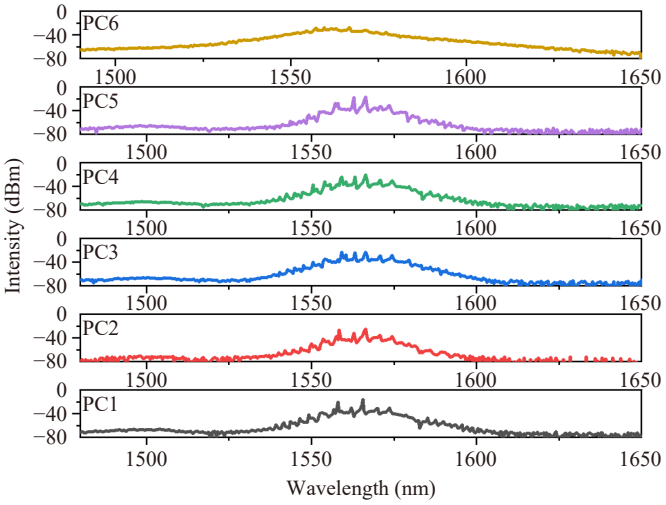

Fig. 6 Spectrum evolution diagrams under different PC states.

Specifically, as the PC was progressively rotated from position PC1 to PC6, the spectrum transitioned from a sharp sideband profile to a smoother distribution, as illustrated in Fig. 6. This behavior arises because adjustments to the PC alter the polarization state within the resonant cavity. Consequently, the loss experienced by certain polarization modes may decrease, while the loss of others may increase due to polarization-dependent attenuation. This redistribution of loss leads to a shift in the dominant polarization mode, ultimately resulting in the observed evolutionary states of the filtered soliton.

At a pump power of 304 mW, fine-tuning of the PC resulted in the generation of a filter-induced noise-like soliton. Mode locking was maintained until the pump power was reduced to 200 mW, at which point it was lost. Figure 7(a) shows the optical spectrum of the output noise-like soliton, which features a central wavelength of 1562.6 nm and a 3-dB bandwidth of 9.8 nm. The oscilloscope trace presented in Fig. 7(b) reveals a pulse interval of 74 ns, corresponding to a fundamental repetition rate of 13.5 MHz and a cavity length of 15 m. The RF spectrum in Fig. 7(c) displays a SNR of 52 dB, confirming stable mode-locked operation. Figure 7(d) presents the autocorrelation trace, which features a broad pedestal with a width of 41.2 ps and a narrow coherent peak superimposed upon it. Fitting the coherent peak yields a pulse width of approximately 305 fs. At an elevated pump power of 304 mW, the intracavity gain is significantly enhanced, and SPM becomes the dominant nonlinear effect. This substantially broadens the spectrum, obscuring the periodic sidebands induced by the Sagnac filter and resulting in a continuous and smooth

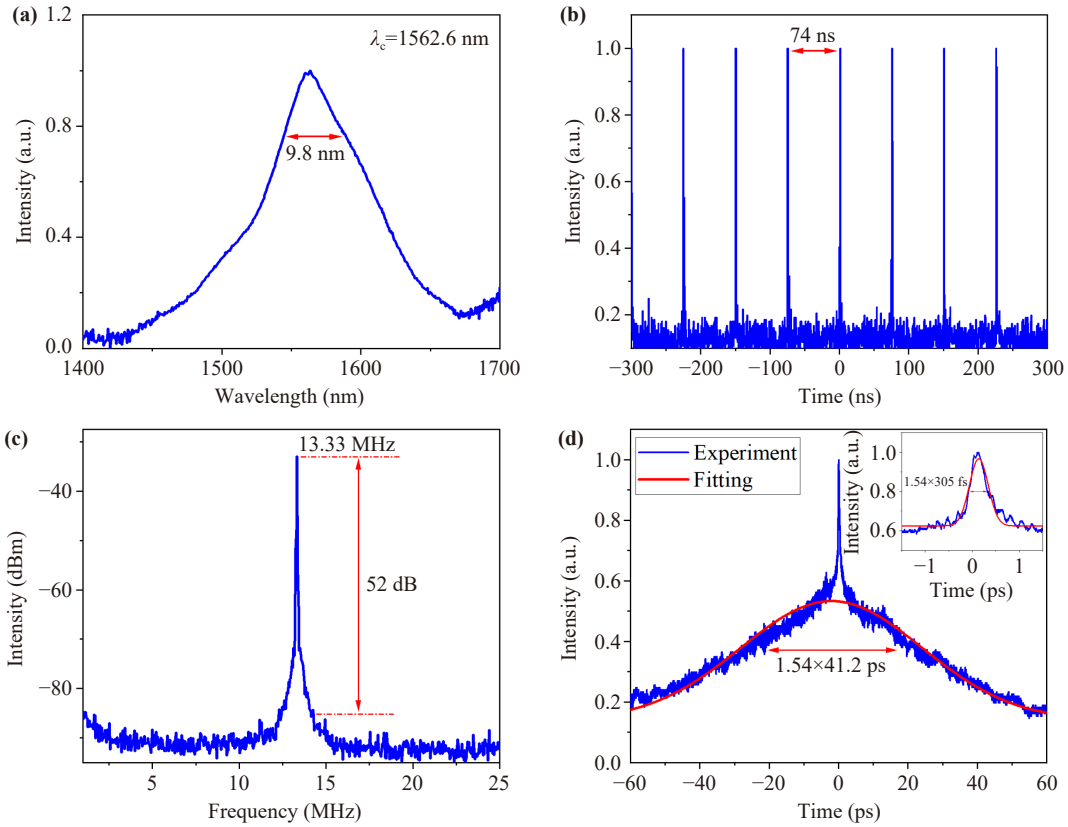

Fig. 7 Output Characteristics of filter-induced noise-like soliton. **(a)** Spectrum; **(b)** Pulse train; **(c)** Radio Frequency (RF) spectrum; **(d)** Autocorrelation curve.

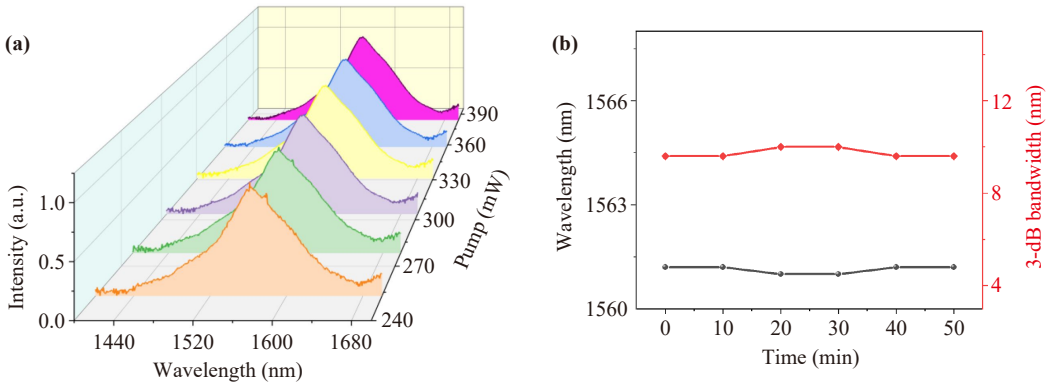

Fig. 8 Output Characteristics of filter-induced noise-like soliton. **(a)** Evolution of spectrum with pump power; **(b)** Stability measurement of central wavelength and 3-dB bandwidth.

spectral profile. Adjusting the PC alters the intracavity phase difference and polarization states, partially suppressing the loss for specific polarization modes. Consequently, the energy originally distributed among discrete sidebands merges into a continuous spectral component, eliminating the spectral basis necessary for forming discrete temporal solitons. According to the Fourier transform duality, a continuous and smooth spectrum corresponds not to discrete solitons in the time domain but rather to a broad temporal pedestal. Owing to their high stability and superior output characteristics, filter-induced noise-like solitons hold significant potential for applications in laser precision machining, optical communications, spectroscopy, and biomedical engineering.

Figure 8(a) illustrates the evolution of the laser spectrum as the pump power is increased from 253 mW to 384 mW. The polarization controller (PC) rotation angle was held constant while the pump power was increased, and spectra were recorded at 30 mW intervals. As shown in Fig. 8(a), the spectrum becomes smoother with increasing pump power, while its overall profile remains unchanged, indicating that the cavity maintains a stable mode-locked state. Figure 8(b) illustrates the central wavelength and 3-dB bandwidth of the output pulses, recorded at 10-minute intervals under a constant pump power of 291.6 mW. Over a 50-minute period, the variations in the central wavelength and 3-dB bandwidth were 0.2 nm and 0.4 nm, respectively, demonstrating the stable operation of the fiber laser. Table 1 compares the performance of recently reported figure-9 mode-locked fiber lasers and Sagnac filters.

4 Conclusion

This study proposes and experimentally demonstrates an erbium-doped fiber laser that integrates a figure-9 cavity with a Sagnac loop. By exploiting the structural properties of the figure-9 cavity based on a NALM and incorporating the filtering effect of the Sagnac loop, stable mode-locked pulse generation was achieved. The high birefringence of the polarization-maintaining fiber (PMF) enables effective optical filtering, and the precise filtering of the Sagnac loop results in strong modulation of the spectral sidebands. The laser exhibits a self-starting threshold of 200 mW. At a pump power of 20.6 mW, a stable filtered soliton centered at 1566 nm was obtained. The output exhibited a repetition rate of 13.5 MHz, a pulse interval of 74 ns, and a SNR of 63 dB. The central

Table 1 Data on figure-9 mode-locked fiber lasers and Sagnac filters in recent years.

Core structure	Signal-to-noise ratio (dB)	Pulse width (ps)	Stability	Center wavelength (nm)	Ref.
Long Loop NALM + Sagnac filter	50	2.7	Power output within 60 minutes ±0.056 mW	1556.4	[19]
9-cavity + chromatic aberration compensation	60	0.2-13.7	Not mentioned	1570	[34]
9-cavity + Sagnac filter	50	0.535	Power output within 120 minutes ±0.027 mW	1027	[21]
Sagnac filter	22.82	Not mentioned	Central wavelength within 12 minutes ±0.068 nm	1562.744	[35]
Sagnac filter integrated 9-cavity	63	0.631	Power output within 50 minutes ±0.003 mW	1566	This work
	52	0.305	Central wavelength within 50 minutes ±0.2 nm	1562.6	

pulse width was measured to be 631 fs, with time separations of 1.49 ps and 1.64 ps between the central peak and its adjacent side peaks. By increasing the pump power to 304 mW and finely adjusting the polarization controller (PC), a filter-induced noise-like soliton was generated, centered at 1562.6 nm with a 3-dB bandwidth of 9.8 nm, an SNR of 52 dB, and a coherent peak width of 305 fs. This passively mode-locked fiber laser features a simple architecture, robust operational stability, and the capability to switch between two distinct filtered soliton states. It holds significant potential for applications in all-optical communication, signal processing, ultrafast laser processing, supercontinuum generation, and low-coherence spectral measurements.

Declarations The authors declare that they have no competing interests and there are no conflicts.

Acknowledgements We are grateful to the International Cooperation Project of Shaanxi Province (No. 2023-GHZD-46), the "Light of the West" Project of the Chinese Academy of Sciences (No. XAB2022YWO6); the Shaanxi Province Sci-Tech Innovation Enterprise Cultivation Program (No. 2023QYPY-06); the 2024 Shaanxi Provincial Department of Education Scientific Research Program-Local Service Special Project: Industrialization Cultivation Project (No. 24JC029); the Start-up Funds of Shaanxi Normal University (Grant Nos. 1112010209 and 1110010717); the Xi'an Municipal Science and Technology Bureau's "Scientists + Engineers" Team Development Project (No. 25KXGC00010); and the Open Research Projects of the State Key Laboratory of Ultrafast Photonics and Technology (No. 2025SKL-uFAST-KF09).

References

1. B. Lu, C. Chen, Q. Lin, Z. Zhang, J. Lang, and J. Bai, Research progress of passively mode-locked ultrashort pulse fiber lasers, *Acta Photonica Sinica* 51(10), 1014003 (2022) (in Chinese)
2. D. Mao, H. Wang, H. Zhang, C. Zeng, Y. Du, Z. He, Z. Sun, and J. Zhao, Synchronized multi-wavelength soliton fiber laser via intracavity group delay modulation, *Nat. Commun.* 12(1), 6712 (2021)
3. X. Jin, Q. Fang, X. Xu, L. Yu, K. Wang, and H. Xia, All-optical control and switching dynamics of dissipative Kerr soliton and perfect soliton crystals, *Ultrafast Sci.* 5, 0088 (2025)
4. X. Li, X. Huang, Y. Han, Enci Chen, P. Guo, W. Zhang, M. An, Z. Pan, Q. Xu, X. Guo, X. Huang, Y. Wang, and W. Zhao, High-performance γ-MnO_2 dual-core, pair-hole fiber for ultrafast photonics, *Ultrafast Sci.* 3(1), 0006 (2023)
5. K. Chi, M. Kong, Q. Yang, X. Liu, and T. Wang, All-fiber ytterbium-doped mode-locked picosecond laser based on semiconductor saturable absorber mirror, *J. Appl. Opt.* 46(1), 217 (2025)
6. X. Zhao, L. Cong, C. Zhang, C. Zhang, I. Ahmad, and B. Fu, Passively mode-locked erbium-doped fiber laser and application in laser thrombolysis, *Photonics* 11(11), 1006 (2024)
7. M. Pal, A. Eber, L. Fürst, E. Hruska, Marcus Ossiander, Birgitta Bernhardt, Phase-locked feed-forward stabilization for dual-comb spectroscopy, *Ultrafast Sci.* 5, 0098 (2025)
8. Y. Han, X. Li, E. Chen, M. An, Z. Song, X. Huang, X. Liu, Y. Wang, and W. Zhao, Sea-urchin-MnO_2 for broadband optical modulator, *Adv. Opt. Mater.* 10(22), 2201034 (2022)
9. X. Li, W. Xu, Y. Wang, X. Zhang, Z. Hui, H. Zhang, S. Wageh, O. A. Al-Hartomy, and A. G. Al-Sehemi, Optical-intensity modulators with PbTe thermoelectric nanopowders for ultrafast photonics, *Appl. Mater. Today* 28, 101546 (2022)
10. H. Afkhamiardakani and J. C. Diels, Mode-locked fiber laser sensors with orthogonally polarized pulses circulating in the cavity, *Sensors (Basel)* 23(5), 2531 (2023)
11. J. Szczepanek, T. M. Kardaś, C. Radzewicz, and Y. Stepanenko, Ultrafast laser mode-locked using nonlinear polarization evolution in polarization maintaining fibers, *Opt. Lett.* 42(3), 575 (2017)
12. A. Malfondet, A. Parriaux, K. Krupa, G. Millot, and P. Tchofo-Dinda, Optimum design of NOLM-driven mode-locked fiber lasers, *Opt. Lett.* 46(6), 1289 (2021)
13. M. Wang, M. Liu, Y. Chen, D. Ouyang, J. Zhao, J. Pei, and S. Ruan, Stable noise-like pulse generation in all-PM mode-locked Tm-doped fiber laser based on NOLM, *Chin. Opt. Lett.* 19, 091402 (2021)
14. S. Wang, Y. Li, Y. Chen, Y. Gao, Z. Zhang, and A. Wang, Femtosecond Nd: fiber laser at 920 nm mode-locked by biased NALM, in: Conference on Lasers and Electro-Optics, OSA Technical Digest, Optica Publishing Group, 2020, paper SW4R.8
15. S. Xiong, D. Luo, Y. Liu, W. Wang, Z. Deng, Z. Tang, G. Xie, L. Zhou, Z. Zuo, C. Gu, and W. Li, Investigation of stable pulse mode-locking regimes in a NALM figure-9 Er-doped fiber laser, *Opt. Express* 31(1), 514 (2023)
16. G. Pu, L. Zhang, W. Hu, and L. Yi, Automatic mode-locking fiber lasers: Progress and perspectives, *Sci. China Inf. Sci.* 63(6), 160404 (2020)
17. S. Kitajima, K. Jung, and N. Nishizawa, 206 MHz fully stabilized all-PM dispersion-managed figure-9 fiber laser comb, *Sci. Rep.* 14(1), 7108 (2024)
18. Y. Xiao, T. Chen, B. Liu, Z. Huang, M. Pang, Y. Leng, and C. Feng, Isolated attosecond free-electron laser based on a subcycle driver from hollow capillary fibers, *Ultrafast Sci.* 5, 0099 (2025)
19. Z. Guo, Q. Hao, J. Peng, and H. Zeng, Environmentally stable Er-fiber mode-locked pulse generation and amplification by spectrally filtered and phase-biased nonlinear amplifying long-loop mirror, *High Power Laser Sci. Eng.* 7, e47 (2019)
20. M. Zhao and T. Wang, Wide spectrum Yb-doped figure-9 fiber laser cavity based on dispersion compensation, *J. Appl. Opt.* 45(4), 834 (2024)
21. J. Ma, M. Ma, H. Liu, and P. P. Shum, Low-noise 2-GHz figure-9 fiber laser based on passive harmonic mode-locking, *Opt. Lett.* 49(22), 6401 (2024)
22. X. Cao, J. Zhou, Z. Cheng, S. Li, and Y. Feng, GHz figure-9 Er-doped optical frequency comb based on

nested fiber ring resonators, *Laser Photonics Rev.* 17(11), 2370053 (2023)
23. X. Li, J. Zhou, Z. Cheng, X. Cao, W. Qi, S. Li, S. Cui, H. Jiang, and Y. Feng, Generation of 978 nm dispersion-managed solitons from a polarization-maintaining Yb-doped figure-of-9 fiber laser, *Opt. Lett.* 48(11), 3051 (2023)
24. X. Liu, S. Lou, Z. Tang, Y. Zhou, H. Jia, and P. Sun, Tunable dual-wavelength ytterbium-doped fiber ring laser based on a Sagnac interferometer, *Optics & Laser Technol.* 116, 37 (2019)
25. X. Huang, X. Guo, X. Huang, F. Peng, X. Li, Z. Wei, and Q. Wang, Highly birefringence-guided microfiber resonator for ultra-high repetition rate ultrashort pulse, *Laser Photonics Rev.* 18(8), 2400166 (2024)
26. M. Kubullek, M. A. Silva-Toledo, R. E. Mainz, F. Scheiba, R. de Q. Garcia, F. Ritzkowsky, G. Maria Rossi, and F. X. Kärtner, Complete electric field characterization of ultrashort multicolor pulses, *Ultrafast Sci.* 5, 0081 (2025)
27. N. Kumar and K. Ramachandran, Dynamic spectral maneuvering by fiber Sagnac loop filter, *Optics & Laser Technol.* 63, 144 (2014)
28. H. R. Zare and S. Shahi, Nonlinear Sagnac filter in eight figure multi-wavelength fiber laser based EDF, *Phys Astron Int J.* 1(3), 84 (2017)
29. X. Jiang, J. Wu, Y. Yang, P. Ting, J. Mao, B. Liu, R. Liu, Z. Yong, C. Qiu, T. Christine, and Y. Su, Wavelength and bandwidth-tunable silicon comb filter based on Sagnac loop mirrors with Mach–Zehnder interferometer couplers, *Opt. Express* 24(3), 2183 (2016)
30. Q. Zhu, Z. Chen, J. Hou, and C. Huang, A fiber temperature sensor based on cascaded FBG and Sagnac interferometer with large measurement scale, in: 21st International Conference on Optical Communications and Networks (ICOCN), Qufu, China, 2023, pp 1–3
31. C. Jiang, Z. Wang, Y. Wan, S. Zhang, L. Yun, B. Sun, C. Mou, Y. Liu, and Z. Zhang, Mode-locked fiber laser with an embedded Sagnac interference filter for strain sensing, *Optics & Laser Technol.* 190, 113161 (2025)
32. G. U. O. Guowen, H. E. Wei, C. H. E. N. Xinyi, Y. A. N. G. Songyan, L. I. Zhihan, and R. E. N. Guanghui, Q-switched erbium-doped fiber laser based on SWNT saturable absorber combined with sagnac filter, *Semicond. Optoelectron.* 44(4), 532 (2023)
33. J. Bogusławski, Ł. Sterczewski, D. Stachowiak, and G. Soboń, Intracavity filtering in SESAM mode-locked fiber lasers: soliton effects and noise performance, *Opt. Express* 31(17), 27667 (2023)
34. J. Li, D. Li, W. Jiang, N. Zhang, Y. Meng, and F. Wang, Pulse duration tunable Figure-9 laser enabled by a composite spectral mode of dissipative soliton, *Opt. Continuum* 3(8), 1334 (2024)
35. Z. M. Chen and C. Q. Huang, Laser temperature sensor based on polarization maintaining fiber and few mode fiber, *Opto-Electron. Eng.* 51(11), 240185–1 (2024)
36. J. Sun, Y. Wang, C. Zhang, L. Xu, and B. Fu, Spatiotemporal nonlinear dynamics in multimode fiber laser based on carbon nanotubes, *Front. Phys. (Beijing)* 19(5), 52201 (2024)
37. C. Zhang, W. Lyu, L. Cong, Z. Gu, Z. Zhang, G. Wang, Y. Lyu, B. Yang, I. Ahmad, and B. Fu, Tunable soliton molecules enabled by a nanotubes-based mode-locked fiber laser, *Front. Phys. (Beijing)* 20(5), 052201 (2025)
38. W. Luo, T. Zhang, X. Li, S. Lv, and D. Duan, Passively mode-locked C-band fiber laser employing carbon nanotubes as saturable absorbers, *Front. Phys. (Beijing)* 20(3), 032205 (2025)